Current Biology, Volume *22*

Supplemental Information

FMNL2 Drives Actin-Based Protrusion and Migration Downstream of Cdc42

Jennifer Block, Dennis Breitsprecher, Sonja Kühn, Moritz Winterhoff, Frieda Kage, Robert Geffers, Patrick Duwe, Jennifer L. Rohn, Buzz Baum, Cord Brakebusch, Matthias Geyer, Theresia E.B. Stradal, Jan Faix, and Klemens Rottner

Supplemental Inventory

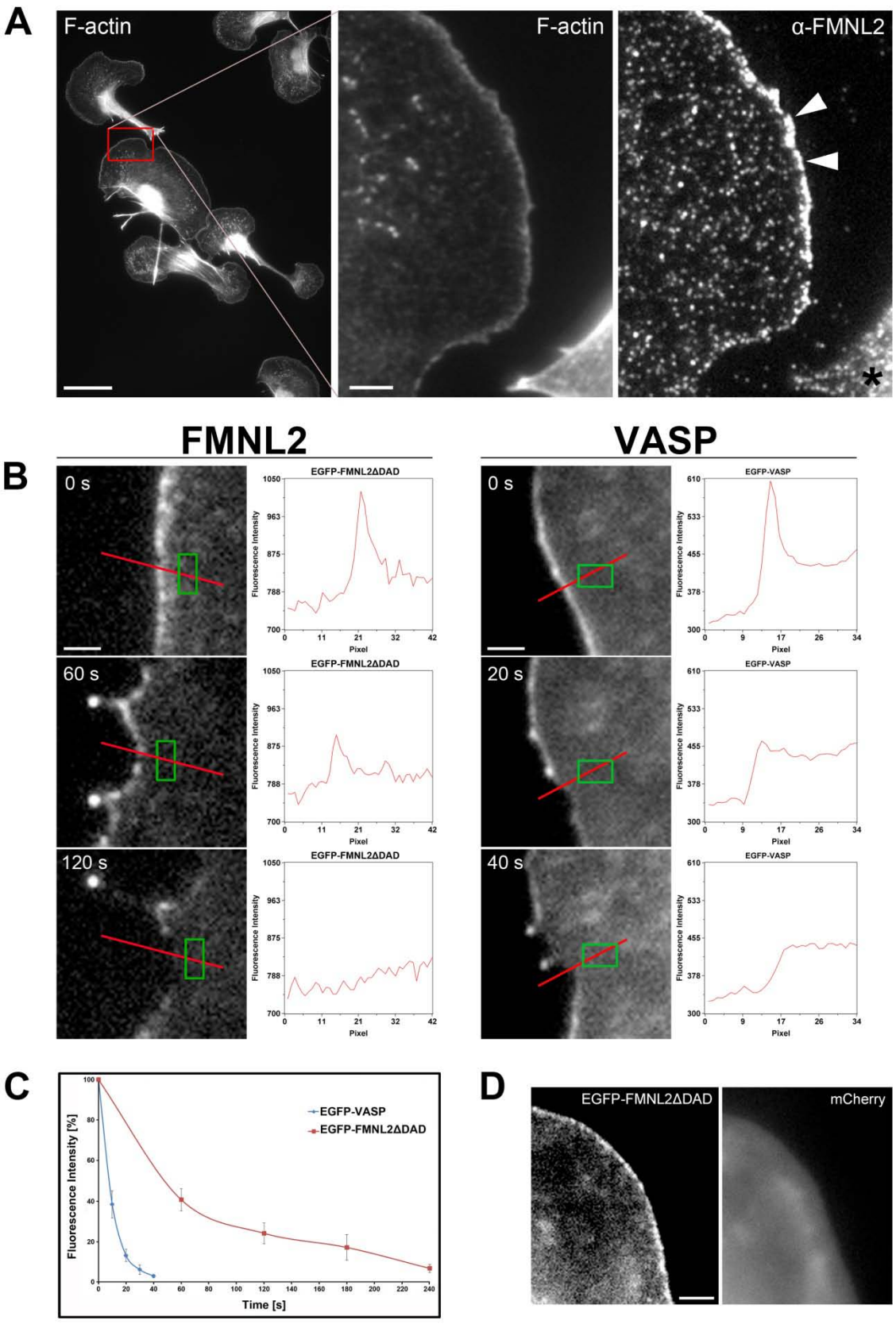
A
F-actin
F-actin
α-FMNL2
B
FMNL2
VASP
0 s
60 s
120 s
0 s
20 s
40 s
EGFP-FMNL2ΔDAD
EGFP-VASP
Fluorescence Intensity
Pixel
C
EGFP-VASP
EGFP-FMNL2ΔDAD
Fluorescence Intensity [%]
Time [s]
D
EGFP-FMNL2ΔDAD
mCherry

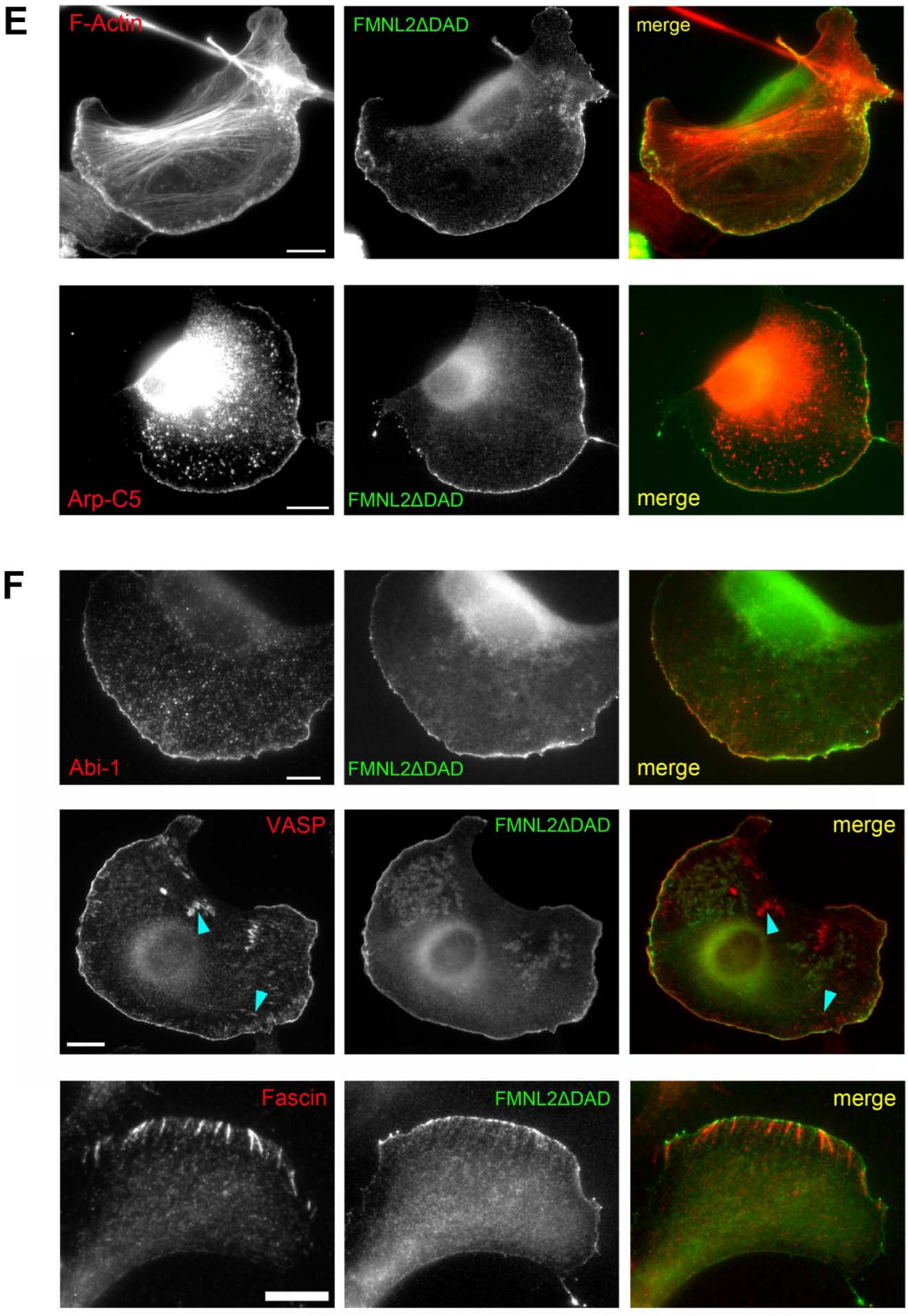
E
F-Actin
FMNL2ΔDAD
merge
Arp-C5
FMNL2ΔDAD
merge
F
Abi-1
FMNL2ΔDAD
merge
VASP
FMNL2ΔDAD
merge
Fascin
FMNL2ΔDAD
merge

Figure S1. FMNL2 Accumulates at the Tips of Canonical Lamellipodia

(A) Zoom-in of the images shown in Figure 1D. Overview of phalloidin staining (left) showing as red inset the region magnified in phalloidin (middle) and α-FMNL2 (right) channels.

(B, C) FMNL2 is more slowly displaced from the lamellipodium tip upon retraction than VASP. B16-F1 cells expressing EGFP-FMNL2ΔDAD (left) or VASP (right) were analyzed prior to and after retraction of the cell periphery. Red lines correspond to intensity scans shown on the right of each image. Green rectangles depict regions of cytoplasm the average intensity of which were subtracted from peak intensities at each time point.

(C) Intensity plot over time showing significantly delayed removal of FMNL2ΔDAD as compared to VASP. Data points and error bars correspond to arithmetic means and standard errors of means (SEM) from at least 20 independent measurements. Bars equal 3µm.

(D) Protruding lamellipodium of a B16-F1 cell co-expressing EGFP-FMNL2ΔDAD and mCherry as volume marker, proving specificity of EGFP-FMNL2ΔDAD accumulation at the lamellipodium tip. Bar, 3µm.

(E) B16-F1 cells plated on laminin and expressing EGFP-FMNL2ΔDAD (green in merge) were counterstained for F-actin (top panel, red in merge) or the Arp2/3-complex subunit Arp-C5 (bottom panel, red in merge). FMNL2ΔDAD accumulates at the front of the lamellipodial actin network. Scale bar, 10µm.

(F) EGFP-FMNL2ΔDAD co-localizes with other lamellipodial tip components, but not with fascin in microspike shafts. B16-F1 cells expressing EGFP-FMNL2ΔDAD (green in merge) were fixed and stained for the WAVE-complex subunit Abi-1 (top, red in merge) or VASP (middle, red in merge) or fascin (bottom, red in merge), as indicated. Both WAVE-complex and VASP show strong overlap with the active formin at the tips of lamellipodia. VASP also targets to focal adhesions, as expected, which are completely devoid of the formin (cyan arrowheads in the middle panel). In addition, in case of broad lamellipodia, EGFP-FMNL2ΔDAD is mostly absent from the lamellipodial actin network, and from the shafts of microspike bundles, highlighted here by counterstaining with the actin-bundling protein fascin. All bars, 10µm.

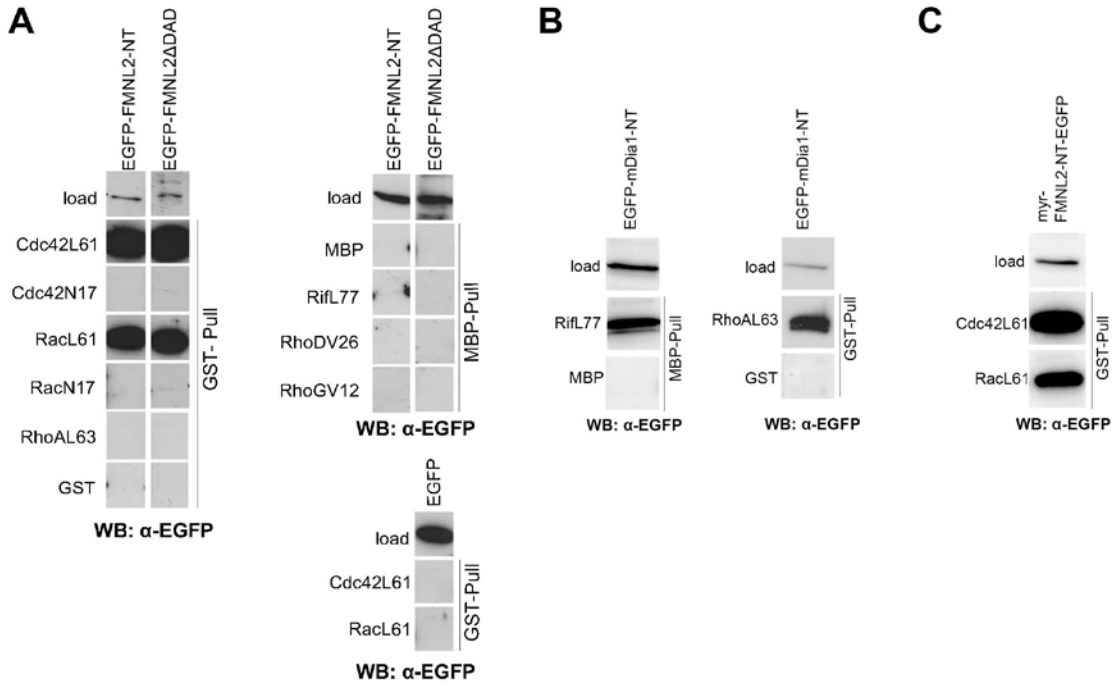
A
EGFP-FMNL2-NT
EGFP-FMNL2ΔDAD
load
Cdc42L61
Cdc42N17
RacL61
RacN17
RhoAL63
GST
GST- Pull
WB: α-EGFP
MBP
RifL77
RhoDV26
RhoGV12
MBP-Pull
WB: α-EGFP
EGFP
load
Cdc42L61
RacL61
GST-Pull
WB: α-EGFP
B
EGFP-mDia1-NT
load
RifL77
MBP
MBP-Pull
WB: α-EGFP
EGFP-mDia1-NT
load
RhoAL63
GST
GST-Pull
WB: α-EGFP
C
myr-FMNL2-NT-EGFP
load
Cdc42L61
RacL61
GST-Pull
WB: α-EGFP

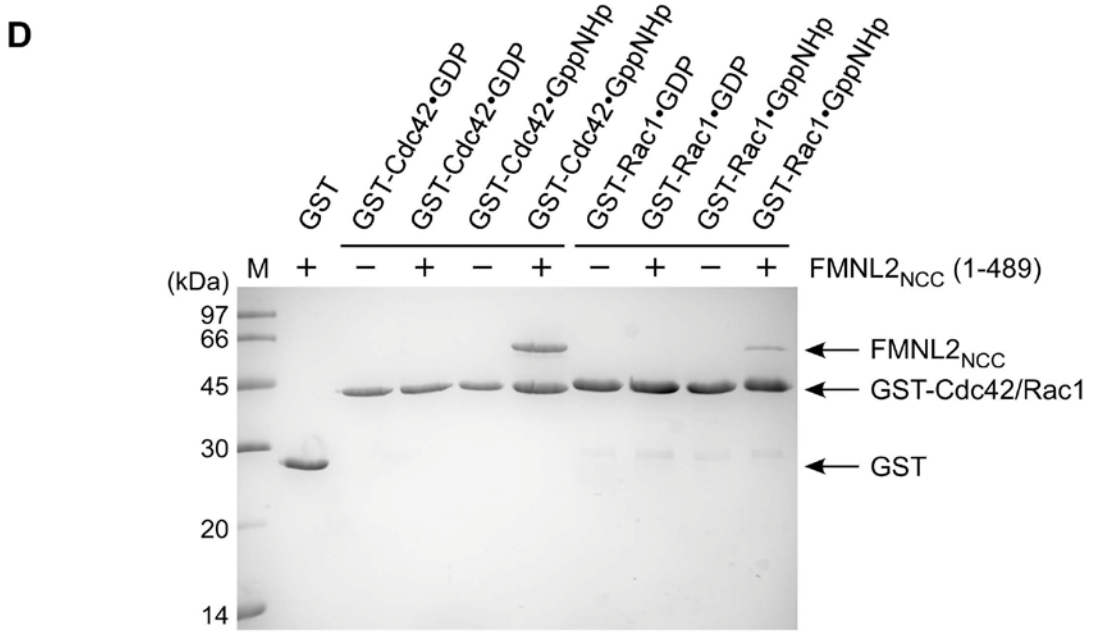
D
GST
GST-Cdc42•GDP
GST-Cdc42•GDP
GST-Cdc42•GppNHp
GST-Cdc42•GppNHp
GST-Rac1•GDP
GST-Rac1•GDP
GST-Rac1•GppNHp
GST-Rac1•GppNHp
M + − + − + − + − + FMNL2NCC (1-489)
(kDa)
97
66
45
30
20
14
FMNL2NCC
GST-Cdc42/Rac1
GST

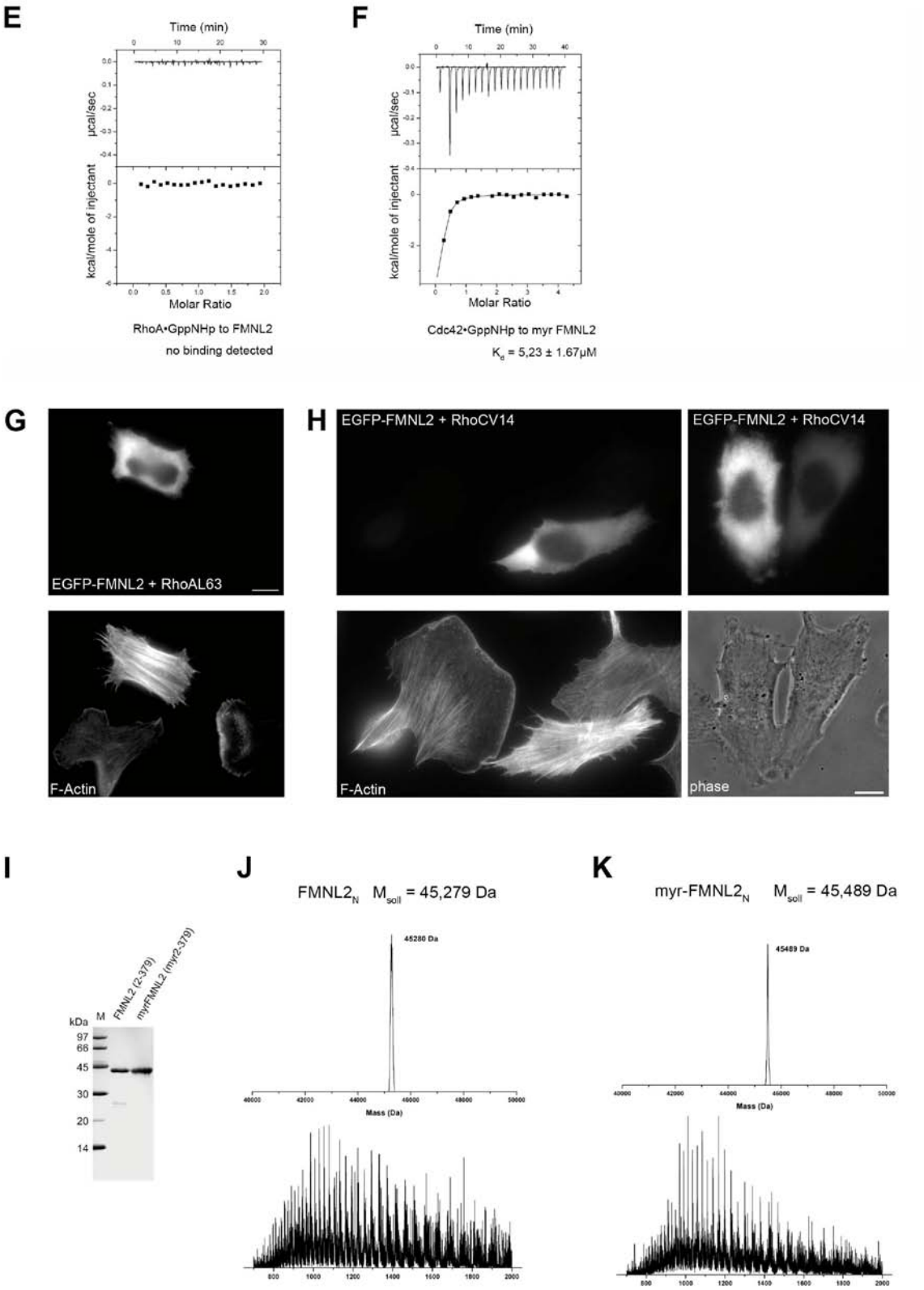
E
Time (min)
µcal/sec
kcal/mole of injectant
Molar Ratio
RhoA•GppNHp to FMNL2
no binding detected
F
Time (min)
µcal/sec
kcal/mole of injectant
Molar Ratio
Cdc42•GppNHp to myr FMNL2
K_d = 5,23 ± 1.67µM
G
EGFP-FMNL2 + RhoAL63
F-Actin
H
EGFP-FMNL2 + RhoCV14
EGFP-FMNL2 + RhoCV14
F-Actin
phase
I
kDa
M
FMNL2 (2-379)
myrFMNL2 (myr2-379)
97
66
45
30
20
14
J
FMNL2_N M_soll = 45,279 Da
45280 Da
Mass (Da)
K
myr-FMNL2_N M_soll = 45,489 Da
45489 Da
Mass (Da)

Figure S2. FMNL2 Is a Potent Cdc42 Interactor and Myristoylated at Its N-Terminus

(A) Pull-downs of EGFP-tagged N-terminus of FMNL2 (EGFP-FMNL2-NT) comprising the GBD and the armadillo repeat subdomain (residues 1-428) or EGFP-tagged FMNL2ΔDAD or EGFP alone ectopically expressed in B16-F1 cells with active and inactive Rho-GTPases as indicated. In these conditions, both FMNL2 variants interacted with constitutively active Cdc42 and Rac1, but not with their dominant negative counterparts (Cdc42N17 and Rac1N17). Neither FMNL2-variant bound constitutively active RhoA (L63), Rif (L77), RhoD (V26) or RhoG (V12). EGFP alone failed to bind constitutively active Cdc42 and Rac1.

(B) Constitutively active Rif and RhoA interact with mDia1. GST-Rif (L77) and MBP-RhoA (L63) beads were probed to pull down an EGFP-tagged variant of their established interaction partner mDia1 (mDia1-NT corresponding to aa 1-427 comprising the GTPase binding domain and the armadillo repeat subdomain) used as control.

(C) Cdc42 and Rac1 interact with an N-terminal fragment of FMNL2 capable of myristoylation. GST-tagged, constitutively active Cdc42 and Rac1 were employed to pull down myristoylatable, ectopically-expressed FMNL2-NT fused to EGFP (myr-FMNL2-NT-EGFP).

(D) Interaction of FMNL2 with Cdc42 and Rac1 is direct, but much weaker in case of Rac1. Pull-downs of purified $FMNL2_{NCC}$ with purified GST-tagged GTPase variants as indicated. As detailed in Experimental Procedures, bait and prey were used in roughly equal amounts (430pmol). Indeed, interaction with GST-tagged Cdc42•GppNHp was observed with a close to 1:1 stoichiometry, whereas the direct interaction with Rac1•GppNHp was significantly weaker.

(E) Active RhoA (RhoA loaded with non-hydrolyzable GppNHp) does not bind to $FMNL2_N$ in isothermal titration calorimetry (ITC) assay.

(F) The N-terminus of FMNL2 (aa 2-379) myristoylated *in vitro* (see below) is capable of binding to Cdc42•GppNHp in ITC. Binding occurred with dissociation constant (K_D) of 5.23±1.67μM. ΔH and TΔS corresponded to -6.98±4.72 and 0.23kcal/mol, respectively, with a molar ratio of 0.14.

(G, H) Constitutively active RhoA and RhoC do not affect the subcellular localization of FMNL2. B16-F1 cells were co-transfected with EGFP-FMNL2 and active RhoA L63 (G) or RhoC V14 (H), fixed and stained for the actin cytoskeleton with phalloidin or subjected to video microscopy (right panel in H). Both RhoA L63 (G) and, to slightly lesser extent, RhoC V14 (H) induced stress fiber formation in B16-F1 cells, but were incapable of effecting the recruitment of EGFP-FMNL2 to the cell periphery. In case of RhoC co-expression, cytosolic localization of EGFP-FMNL2 was confirmed by both fluorescence and phase-contrast video microscopy (H, right panel). Scale bars correspond to 10μm.

(I-K) Generation of recombinant, myristoylated $FMNL2_N$.

(I) SDS PAGE analysis of FMNL2 (2-379) and myristoylated FMNL2 (2-379) showing the homogeneity of the protein samples. The gel was stained with Coomassie blue.

(J, K) Mass spectrometry analysis of non-myristoylated (J) and myristoylated $FMNL2_N$ (K). Covalent modification of the N-terminus of FMNL2 with the myristic moiety leads to an increase in mass of 209 Da. The experimentally determined masses of 45,280 Da and 45,489 Da fit very well to the calculated masses (M_{soll}) of 45,279 Da and 45,489 Da for non-myristoylated and myristoylated $FMNL2_N$, respectively.

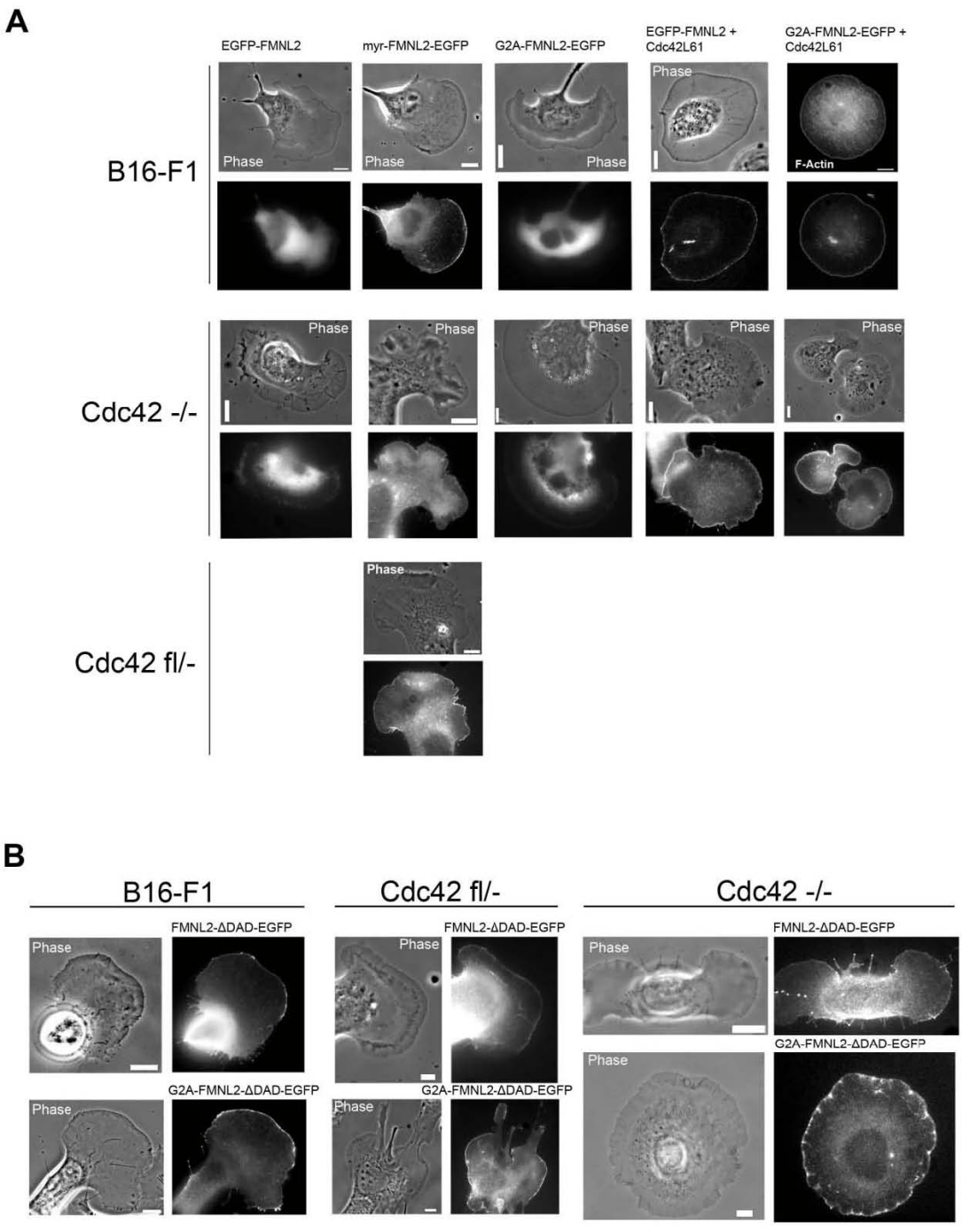
A
EGFP-FMNL2
myr-FMNL2-EGFP
G2A-FMNL2-EGFP
EGFP-FMNL2 + Cdc42L61
G2A-FMNL2-EGFP + Cdc42L61
B16-F1
Cdc42 -/-
Cdc42 fl/-
Phase
F-Actin
B
B16-F1
Cdc42 fl/-
Cdc42 -/-
FMNL2-ΔDAD-EGFP
G2A-FMNL2-ΔDAD-EGFP
Phase

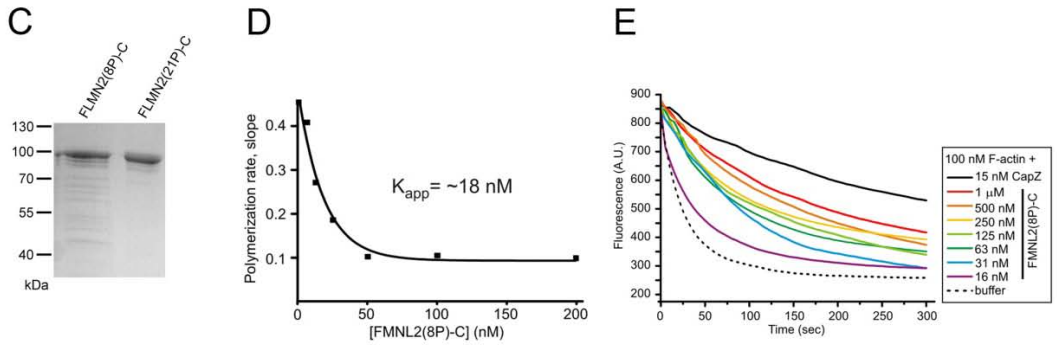
C
FLMN2(8P)-C
FLMN2(21P)-C
130
100
70
55
40
kDa
D
Polymerization rate, slope
0.4
0.3
0.2
0.1
K_{app}= ~18 nM
0
50
100
150
200
[FMNL2(8P)-C] (nM)
E
Fluorescence (A.U.)
900
800
700
600
500
400
300
200
0
50
100
150
200
250
300
Time (sec)
100 nM F-actin +
15 nM CapZ
1 μM
500 nM
250 nM
125 nM
63 nM
31 nM
16 nM
buffer
FMNL2(8P)-C

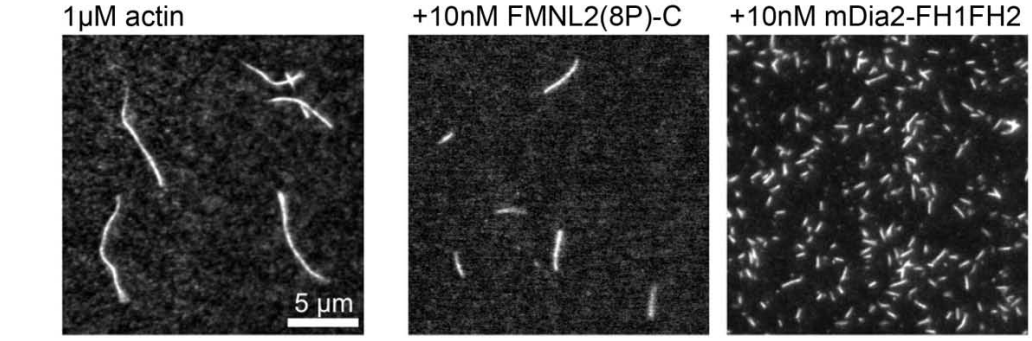
F
1μM actin
+10nM FMNL2(8P)-C
+10nM mDia2-FH1FH2
5 μm

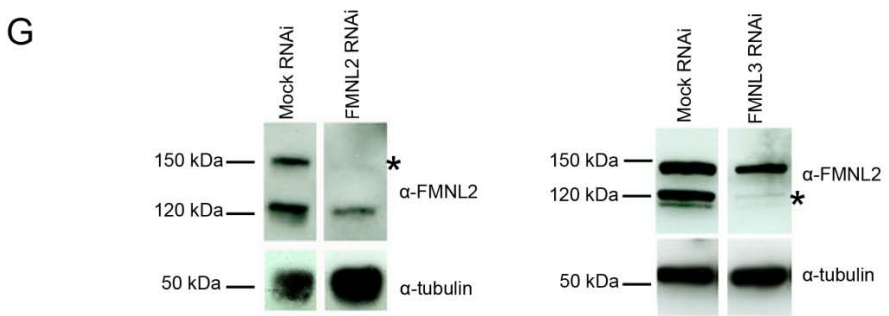
G
Mock RNAi
FMNL2 RNAi
150 kDa
120 kDa
50 kDa
*
α-FMNL2
α-tubulin
Mock RNAi
FMNL3 RNAi
150 kDa
120 kDa
50 kDa
α-FMNL2
*
α-tubulin

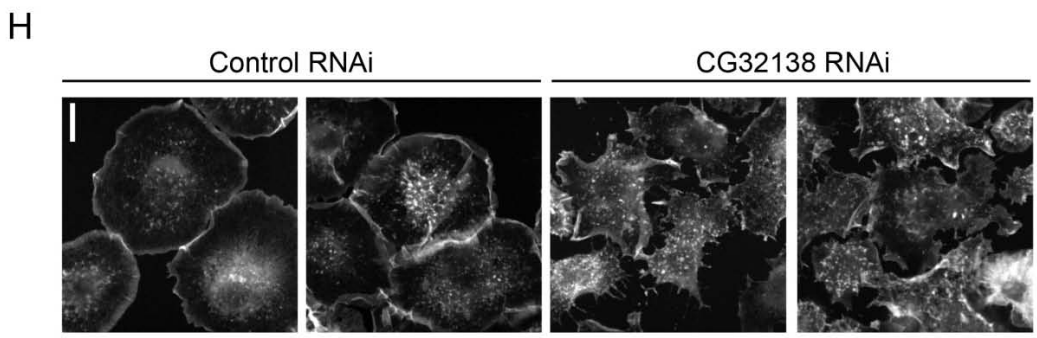
H
Control RNAi
CG32138 RNAi
I

Figure S3.

(A, B) Relative roles of myristoylation and Cdc42 in subcellular FMNL2 positioning. Comparison of localization of FMNL2-variants as indicated in B16-F1 cells (genotype $Cdc42^{wt/wt}$), Cdc42-expressing control fibroblasts ($Cdc42^{fl/-}$) or Cdc42-deficient fibroblasts ($Cdc42^{-/-}$) with or without ectopic co-expression of constitutively, active Cdc42 (L61). Images show representative examples of localization of constructs classified for the table shown in Figure 2G. Phase-contrast images reveal overall morphology of the cells and the presence at the cell periphery of lamellipodia, filopodia or retractile edges. All images correspond to live cells. Bars equal 10µm in all cases.

(C) Coomassie gel of purified FMNL2(8P)-C and FMNL2(21P)-C as indicated.

(D) Plot showing dependence of polymerization rate (slopes from measurements in Figure 3A) on concentration of FMNL2(8P)-C. K_{app} corresponds to the apparent inhibition constant as detailed in Experimental Procedures.

(E) FH1-FH2 of FMNL2 inhibits dilution-induced depolymerization of actin filaments *in vitro*. 5µM F-actin (23% pyrene-labeled) were diluted to 100 nM in 1 x KMEI-buffer containing FMNL2(8P)-C or CapZ at the concentrations indicated. The decrease in F-actin fluorescence was monitored over time.

(F) Generation of filaments by mDia2 *versus* FMNL2. TIRFM micrographs of 1 µM actin (23% OG-labeled) polymerized either alone or in the presence of FMNL2(8P)-C or mDia2-FH1FH2 for 250 seconds show that mDia2 drastically increases the number of filaments, while FMNL2 lacks such activity.

(G) Monoclonal α-FMNL2 antibody detects two different protein products migrating at molecular weights of 150 and 120kDa. Sequence comparisons revealed the possibility that the rapidly migrating species (120kDa) corresponds to endogenous FMNL3. This was demonstrated using RNA interference. B16-F1 cells transfected with a construct mediating knockdown of FMNL2 specifically displayed reduced expression levels of the 150kDa protein (left, asterisk, see also Figure 4A), indicating that the 150kDa protein represents FMNL2. In contrast, knockdown of FMNL3 erased the lower molecular weight band (right panel, asterisk). Crossreaction of the antibody with FMNL3 was also confirmed using EGFP-tagged FMNL3 (data not shown). α-tubulin was used as a loading control.

(H) FMNL knockdown in *Drosophila* S2R+ cells affects lamellipodial integrity. Analysis of control and CG32138 RNAi-treated *Drosophila* S2R+ cells stained for the actin cytoskeleton with phalloidin. Control *Drosophila* S2R+ cells seeded on FBS-coated coverslips display broad lamellipodia homogenously protruding around the entire cell periphery (two representative panels on the left). In contrast, knockdown of CG32138 (right panels), the sole fly ortholog of FMNL, causes disorganization of the cell periphery with less continuous or “broken” lamellipodial protrusions. Scale bar, 10µm.

Supplemental Experimental Procedures

Cells and Transfections

B16-F1 (mouse melanoma; CRL-6323) and VA-13 (human lung fibroblast SV-40 transformed; CCL-75.1) cells were purchased from the American type culture collection and cultured as described [1]. $Cdc42^{fl/-}$ and $Cdc42^{-/-}$ cells were maintained as described [2]. NIH 3T3 (murine embryonal fibroblast; CRL-1658), Swiss 3T3 (murine embryonal fibroblast; CCL-92), A431 (CRL-1555), CaCo2 (colorectal adenocarcinoma; HTB-37) and Hela S3 cells (human cervix adenocarcinoma; CCL-2.2) were cultured in DMEM, 10% FCS (Sigma-Aldrich Co.), 2mM glutamine, 0.1mM nonessential amino acids and 1mM sodium pyruvate (all Invitrogen). Cells were transfected using Superfect (Qiagen) and Fugene 6 (Roche) for B16-F1 and Cdc42 control or -KO cells, respectively.

S2R+ *Drosophila* cells were cultured in Shields and Sang M3 insect medium (Sigma-Aldrich Co.) substituted with 10% heat-inactivated fetal bovine serum (PAA) and antibiotics (1% P/S, Sigma-Aldrich Co.).

DNA Constructs

For cloning of FMNL2 cDNA, total mRNA was isolated from Hela S3 cells and subjected to reverse transcription using Omniscript reverse transcriptase Kit (Qiagen) according to manufacturer's instructions. Full length, human FMNL2 (NCBI reference sequence: NP_443137.2), corresponding to FMNL2B in Figure 1C, was engineered by fusion of a cDNA clone (IRALp962K1959Q2) harboring a C-terminally truncated FMNL2 variant (bp 1-1088) with PCR-derived and custom-synthesized cDNA-fragments. The cDNA clone (bp 1-1088) was amplified by PCR using primers 5'-GAGGTCGACATGGGCAACGCAGGGAGCA-3' & 5'-TCCCGAACGACATCCAGCTC-3' and fused to fragment 1089-1470 amplified from Hela S3 cDNA using primers 5'- GACAAGCTTCAAGTCCAGATCC-3' & 5'-ATGGACAATGTGCCAGAAGC-3'. Codon-optimized fragment 1471-1953 was synthesized by Genescript (Piscataway, NJ) and fragment 1954-3279 again amplified from Hela S3 using primers 5'- AAGCCCAATCAGATCAATGG -3' & 5'-GAGACCGCGGTCACATTGTTATTTCGGCA-3'. The C-terminus encoding FMNL2 splice variant B (Figure 1C) was synthesized by Genescript and exchanged for the C-terminus derived from Hela S3 cDNA using BamH1 and SacII restriction enzymes. For generation of EGFP-tagged FMNL2, the full length cDNA was fused into EGFP-C3 (Clontech) using *Xho*I/*Sac*II restriction enzymes. Site directed mutagenesis was carried out using Qiagen site directed mutagenesis kit employing forward primer 5'-TGCAGTCGACATGGCCAACGCAGGGAGCATGG-3' and the respective complementary sequence as reverse primer.

All truncated variants of FMNL2 were cloned by PCR amplification with respective primers using EGFP-FMNL2 as template. All constructs were sequence-verified.

For expression of the two C-terminal FLMN2 constructs carrying 8 or 21 consecutives proline residues in the FH1 domain, the corresponding DNA fragments were amplified by PCR and cloned into SalI and NotI sites of pGEX-6P-3 (Amersham Pharmacia Biotech, Piscataway, NJ). FLMN2-8P-FH1-FH2-C [designated FMNL2(8P)-C in Fig 3] was amplified from human cDNA using forward primer 5'-CGCGTCGACCCACCTCCCCCACCGCCTCCACCCCTGCCCGGGCCCGCAGCTGAG-3' and reverse primer 5'-CGCGCGGCCGCTCACATTGTTATTTCGGCACCATTAAC-3'. FLMN2-21P-FH1-FH2-C [short FLMN2(21P)-C] was amplified from a synthetic FLMN2 cDNA (Genescript, Piscataway, NJ) with an optimized codon usage for proline residues using forward primer 5'-CGCGTCGACATGCCTCCGCCCCCACCCCCGCCT-3' and as reverse primer the same one as given above for FMNL2(8P)-C. FMNL2(8P)-C and FLMN2(21P)-C corresponded to residues 566-1092 and 552-1092 of FMNL2-B (Figure 1C).

For expression of mDia2-FH1FH2, an mDia2 fragment was amplified from human cDNA using primers 5'-CGCGGATCCGTGCCTCCACCACCTCCCCTGGGA-3' &

5’-GCGGTCGACTCATGTCTCATCACCCTCAGTCTTCATTTC-3’ and fused into pGEX-6P-1 (Amersham) with BamHI and SalI. The expressed FH1FH2-fragment corresponded to residues 610-1077.

The WAVE1-VCA (WCA) fragment encoding residues 491-559 was amplified from human brain cDNA (Invitrogen) using primers 5’-CGCGGATCCCCTGTAATCAGTGATGCCAGGAGT-3’ & 5’-CGCGTCGACTTACTCCAACCAATCTACTTCATC-3’, and ligated into the BamHI and SalI sites of pGEX-6-P1 (GE Healthcare). The mCherry expression vector was obtained by exchanging EGFP in EGFP-C1 (Clontech) for mCherry [3], a kind gift from Roger Tsien (University of California at San Diego, La Jolla, USA). EGFP-VASP was as described [4].

3 x HA-tagged, constitutively active, human RhoC (V14) in pcDNA3.1+ was purchased from Missouri S&T cDNA Resource Center (Rolla, MO, USA). pRK5-myc-Cdc42L61 and pRK5-myc-Rac1L61 were gifts from Laura Machesky (Beatson Institute, Glasgow, UK). pGex2T-Cdc42L61, pGex2T-Cdc42N17, pGex2T-Rac1L61 and pGex2T-Rac1N17 were kindly provided by Alan Hall (Memorial Sloan-Kettering Cancer Center, New York, USA). pEGFP-RhoDV26, pRK5-myc-RifL77 and pcDNA3.1+3xmyc-RhoGV12 were provided by Pontus Aspenström (Karolinska Institute, Stockholm, Sweden), and used to clone cDNAs encoding respective GTPases into pMal-C2X.

For ITC measurements and pull downs with purified proteins, two FMNL2 expression constructs were engineered with domain boundaries 1-379 and 1-489, respectively, designated as FMNL2$_{N}$ and FMNL2$_{NCC}$. Coding sequences were amplified from human FMNL2 by PCR using primers harboring *Nco*I and *Hind*III restriction sites at the 5' and 3' ends, respectively. The fragments were cloned into the pET-23d expression vector (Novagene) that contained a C-terminal His$_{6}$-tag for affinity chromatography, and to potentially allow N-terminal myristoylation upon co-expression with the N-myristoyl transferase in bacterial cells (see below).

Antibodies, Immunolabeling and Video Microscopy

For immunolabelings, B16-F1 cells were seeded onto glass coverslips coated with laminin (25µg ml^{-1}, Sigma-Aldrich Co., St. Louis, MO, USA), and fixed and stained as described [1].

Monoclonal anti-FMNL2 (ab57963) antibody was purchased from Abcam (Abcam, UK). Monoclonal anti-GFP (101G4B2) and monoclonal anti-α-tubulin (clone 3A2) antibodies were obtained from Synaptic Systems (Göttingen, Germany). Monoclonal anti-Abi (W8.3) antibody was kindly provided by Giorgio Scita, Milan, Italy [5]. Monoclonal anti-fascin antibody (55K2) was from Santa Cruz Biotechnology Inc. (Santa Cruz, CA, USA). Monoclonal anti Arp-C5 [6] and polyclonal anti VASP [7] were as described. Alexa Fluor 594 and Alexa Fluor 350-coupled phalloidin and secondary antibodies were purchased from Invitrogen (Germany).

Drosophila cells were fixed, extracted and stained with TRITC-conjugated phalloidin following standard protocols. Coverslips were mounted in FluorSaveTM Reagent (Calbiochem) and imaged on a Leica SP5 confocal microscope.

Live cell imaging was done with B16-F1 cells seeded on laminin-coated coverslips or Cdc42$^{-/-}$ and Cdc42$^{+/-}$ cells plated on fibronectin (Roche; 25 µg/ml). Cells were observed in an open heating chamber (Warner Instruments, Reading, UK) with a heater controller (Model TC-324 B, SN 1176) at 37°C. B16-F1 cells were maintained in F12 HAM HEPES-buffered medium (Sigma-Aldrich Co.) including complete supplements. Cdc42$^{-/-}$ and Cdc42$^{+/-}$ cells were observed in regular growth medium including 25mM HEPES.

Light microscopy was performed on an inverted microscope equipped with electronic shutters, a filter wheel (LUDL Electronic Products LTD, SN: 102691 and driver SN: 1029595) and standard epifluorescence illumination (light source HXP 120, Zeiss). Live cell images were obtained with 63x/1.4NA, 100x/1.4NA or 40x/1.3NA Plan apochromatic objectives. Triple stainings were performed using 63x/1.25NA or 100X/1.3 NA Plan-Neofluar objectives. Images were acquired with a back-illuminated, cooled, charge-coupled-device (CCD) camera (TE-CCD 800PB, CoolSnap K4 or CoolSnap HQ2, Princeton Scientific Instruments, Princeton, USA)

driven by IPLab (Scanalytics Inc., Fairfax, USA) or MetaMorph software (Molecular Devices, Sunnydale, USA). Data were processed using MetaMorph, Photoshop and ImageJ.

Qualitative assessment of lamellipodial accumulation of FMNL2 constructs in different cell types as summarized in Figure 2G was exclusively done by live-cell imaging experiments (representative images shown in Figure S3A, B). At least 7 cells were analyzed for each condition. Categorization was a detailed in the legend to Figure 2G.

Displacement analysis of FMNL2 (compared to VASP) upon retraction was performed as follows: B16-F1 cells transiently expressing EGFP-FMNL2ΔDAD or EGFP-VASP were seeded on laminin and subjected to widefield video microscopy as described above. Images were captured every 15 and 10 seconds, respectively, to avoid excessive bleaching. Movies were then screened for protrusion events followed by retraction, and fluorescence intensity changes at the cell periphery during such events analyzed using linescans. Frames immediately before retraction were defined as time zero and changes in fluorescence intensity monitored over time as shown in Figure S1B. For quantifications (Figure S1C), peak fluorescence intensities from line scans at time zero were subtracted from cytosol regions behind the lamellipodium, and normalized to 100%. Intensities at later time points were treated in an identical fashion, and expressed relative to the peak fluorescence at time zero. At least 20 individual retraction events were analyzed for each construct.

RNA Interference

RNAi in mammalian cells was done using vectors driving expression of short hairpin (sh) RNAs. RNAi-vectors were purchased from InvivoGen (Toulouse, France). Targeting sequences effecting knockdown of FMNL2 or FMNL3 were 5'-GGAAGTCTGCGGATGAGATAT-3' and 5'-GGTGCAGATTCAAGCGTACCT-3', respectively. Targeting sequences were fused into the pSiRNA-h7SK vector backbone encoding a GFP variant. A vector harboring a scrambled sequence was used as RNAi control. For knockdowns, B16-F1 cells were co-transfected using FuGene6 (Roche) with the respective knockdown vector and a plasmid conferring puromycin resistance (pPUR, Clontech). Puromycin was added 24h after transfection, and removed prior to respective analyses. All analyses were performed 4 days after transfection of respective constructs. Protein rundown was verified by Western Blotting.

RNAi experiments in *Drosophila* were performed as described previously [8]. The dsRNA targeting CG32138 was prepared using primers corresponding to BKN21754 (see http://rnai2.dkfz.de/GenomeRNAi/reagentdetails/BKN21754) to amplify a 527 bp-fragment and wildtype *Drosophila* genomic RNA as template. The PCR product was used to create dsRNA employing the MegaScript T7 kit (Ambion), and processed according to standard procedures [9]. dsRNA targeting LacZ was used as negative control. After dsRNA addition, cells were grown for 6 days at 24ºC, replated onto FBS-coated coverslips and allowed to spread before analysis.

Cell Migration Assays and Determination of Lamellipodial Protrusion Rates

Lamellipodium protrusion was measured with B16-F1 cells seeded subconfluently on glass coverslips coated with laminin. Protrusions were recorded over a time period of at least 10 min acquiring images every 5s. Measurements were carried out as indicated in Figure 4B. Data were processed and analyzed using Excel, Sigma Plot, OriginPro and Minitab 5.0.

Cell migration assays were performed with B16-F1 cells plated subconfluently into 6 well-plates. 48 h after plating, cells were recorded with an AxioCam MRm camera on an Axiovert 200 automatic microscope equipped with closed heating and CO_2 perfusion devices (Carl Zeiss, Jena, Germany) over a time period of 24 h, with time intervals of 15 min between frames. Migration analyses were carried out using the track objects function of Metamorph (Molecular Devices Corp, Downingtown, PA, USA). Data were logged into Excel files and processed using Excel 2003 (Redmond, WA, USA) and Sigma Plot 10.0.

Protein Purification, Pulldown Assays, and Mass Spectrometry

GST-tagged proteins were expressed in Rosetta and purified using glutathione-Sepharose resin (Amersham Pharmacia Biotech) by standard procedures. Arp2/3-complex was purified from bovine brain by affinity chromatography employing GST-VCA coupled to CNBr-sepharose essentially as described [10]. The concentration of Arp2/3 complex was determined spectrophotometrically using an extinction coefficient of 224,480$M^{-1}cm^{-1}$ at 280 nm, derived from the amino acid sequence of the seven polypeptides of the complex. The expression and purification of human profilin I was as described [11].

For pull-downs, recombinant GST- or MBP-tagged Rho-GTPases were expressed and purified following protocols from GE Healthcare. Different GTPases were purified in buffer A (50mM Tris, pH 7.5, 50mM NaCl, 5mM $MgCl_2$, Complete Mini™ protease inhibitor cocktail tablets, EDTA-free [Roche]), snap frozen and stored at -70°C coupled to glutathione-Sepharose (GE Healthcare) or amylose resin beads (NEB) at a concentration of 2-5mg protein per ml slurry. N-terminal FMNL2 fragments ($FMNL2_N$ and $FMNL2_{NCC}$) were expressed in *Escherichia coli* strain Rossetta (DE3) with a C-terminal 6xHis-Tag at 27°C, and purified by nickel affinity chromatography following standard protocols. Proteins were aliquoted and stored at -80°C in 20 mM Tris/HCl pH 8.0, 500 mM NaCl, 10% glycerol, 1 mM dithioerythreitol. N-myristoylation of the FMNL2-fragment used in ITC-assays (myr$FMNL2_N$) was achieved in *E. coli* bacterial cells by co-expression of $FMNL2_N$ expression plasmid with N-myristoyl transferase and addition of myristic acid as co-enzyme essentially as described for HIV-1 Nef [12]. For pull-downs of expressed proteins, B16-F1 cells were grown in 10cm dishes, washed with PBS and lysed in 300µl lysis buffer (15mM KCl, 50mM NaCl, 8mM Tris base, 12mM HEPES, 5mM $MgCl_2$, 1% Triton X-100, Complete Mini™ protease inhibitor cocktail tablets [Roche]). Cell lysates were incubated with 30µl of respective GTPase-coupled beads for 1h at 4°C. Samples were washed three times with wash buffer (lysis buffer without Triton X-100) and subjected to SDS-PAGE and Western Blotting.

For the *in vitro* pull-down shown in Figure S2D, 430 pmol of the respective GST-tagged GTPase was loaded onto glutathione–Sepharose beads (GE Healthcare), and incubated with 430 pmol $FMNL2_{NCC}$ in 275µl binding buffer (20 mM Tris, pH 8.0, 150 mM NaCl, 10% Glycerol, 0.005% Triton-X, 1 mM beta-mercaptoethanol) for 30 min at 4°C. Beads were washed four times with 250µl binding buffer and resuspended in 20µl SDS loading buffer. Binding interactions were analyzed by SDS-PAGE and Coomassie staining (8µl of each sample loaded on 18% -gel).

Rho GTPases used for ITC measurements were expressed as GST fusion proteins from *E. coli* using C-terminally truncated protein variants to omit the membrane binding anchor. RhoA 1-193, Rac1 1-177 and Cdc42 1-179 were dialyzed against ITC puffer and typically concentrated to 10 mg/ml. Cleavage of GST by TEV protease and nucleotide exchange was performed essentially as described [concentrated to 10 mg/ml. Cleavage of GST by TEV protease and nucleotide exchange was performed essentially as described [concentrated to 10 mg/ml. Cleavage of GST by TEV protease and nucleotide exchange was performed essentially as described [13].

Pyrene-Actin Assays

Actin polymerization was measured by fluorescence spectroscopy in a Fluoroskan II plate reader (Thermo Scientific, Waltham, MA) with pyrene-labeled actin in KMEI-buffer (50 mM KCl, 2 mM $MgCl_2$, 2 mM EGTA, and 20 mM imidazole, pH 7.3) as described [14]. For quantitative comparison of polymerization rates shown in Figure S3D, slopes for each curve were obtained by measuring average slopes between 900 and 1200 seconds of the reactions in Figure 3A, and plotted as a function of FMNL2 concentration. The concentration of FMNL2(8P)-C required to obtain 50% inhibition of actin polymerization, defined as apparent inhibition constant (K_{app}), was determined by fitting the data to a single exponential decay function, yielding a value of 18 nM.

TIRF Microscopy

Time-lapse evanescent wave fluorescence microscopy with Oregon-green (OG)-, Alexa-488- or Atto-488-labeled actin was essentially performed as described [14]. In brief, images from an Olympus IX-81 inverted microscope were captured every 5 s with exposure times of 200 ms with a Hamamatsu Orca-R2 CCD camera (Hamamatsu Corp., Bridgewater, NJ). The pixel size corresponded to 0.11 µm. The elongation rates of filaments were calculated with ImageJ software using the plugins MtrackJ and Manual Tracking. Each experiment was repeated at least three times. For determination of the elongation rates shown in Figure 3D, numbers of individually analyzed filaments were as follows: actin alone: 45, FMNL2(8P)-C alone: 21, FMNL2(8P)-C + profilin: 13, FMNL2(21P)-C + profilin, 8 filaments. For determining the elongation rates shown in Figure 3H, at least 10 individual filaments were analyzed for each condition. For comparison of nucleation efficacies, the average number of filaments was obtained by counting actin filaments in an area of 100 x 140 µm 420 s after initiation of the polymerization reaction.

Isothermal Titration Calorimetry

Isothermal titration calorimetry (ITC) experiments were performed in ITC buffer (20 mM Tris/HCL, pH 8.0, 150 mM NaCl, 1 mM DTE, 5 mM $MgCl_2$) at 25° C using a MicroCal iTC200 micro-calorimeter (GE Healthcare). Prior to the titration experiments, $FMNL2_N$ proteins and small GTPases were equilibrated in ITC buffer by dialysis and exhaustively degassed. For all reactions, a solution of 250 to 500 µM GTPase was injected in 19 steps of 2 µl volume to a solution of 25 to 50 µM $FMNL2_N$ placed in the measurement cell. Each titration experiment was corrected by a control titration of the ligand into ITC buffer. Data were analyzed using the software provided by the manufacturer.

DNA Microarray Hybridization and Analysis

Microarray analyses using AffymetrixTM genechips as shown in Figure 1A were done as follows: Quality and integrity of total RNA was controlled on Agilent Technologies 2100 Bioanalyzer (Agilent Technologies; Waldbronn, Germany). 500 ng of total RNA were used for biotin labeling according to the 3´ IVT Express Kit (Affymetrix; Santa Clara, CA). 7.5 µg of biotinylated cRNA were fragmented and placed in a hybridization cocktail containing four biotinylated hybridization controls (BioB, BioC, BioD, and Cre) as recommended by the manufacturer. Samples were hybridized to an identical lot of Affymetrix GeneChip MOE 430 2.0 for murine and HG U133 2.0 for human samples for 16 hours at 45°C. Steps for washing and SA-PE staining were processed on the fluidics station 450 using the mini_euk2v3_FS450 protocol (Affymetrix; Santa Clara, CA). Image Analysis was performed on a GCS3000 Scanner equipped with GCOS1.2 Software Suite (Affymetrix; Santa Clara, CA).

Statistical Analyses

To test for meaningful differences of experimental samples in random migration assays or lamellipodial protrusion rate measurements, statistical analyses were carried out using Sigma plot (SPSS, Chicago, IL), OriginPro and Minitab 5.0 software. Data derived from an appropriate number of experiments as indicated in figure legends. Normality analyses were performed according to Shapiro-Wilk. Since data not always appeared normally distributed, datasets were routinely compared using the non-parametric Mann-Whitney Rank Sum test. A probability of error of 5% ($p<0.05$) was considered to indicate statistical significance.

Supplemental References

1. Block, J., Stradal, T.E., Hanisch, J., Geffers, R., Kostler, S.A., Urban, E., Small, J.V., Rottner, K., and Faix, J. (2008). Filopodia formation induced by active mDia2/Drf3. J Microsc *231*, 506-517.

2. Czuchra, A., Wu, X., Meyer, H., van Hengel, J., Schroeder, T., Geffers, R., Rottner, K., and Brakebusch, C. (2005). Cdc42 is not essential for filopodium formation, directed migration, cell polarization, and mitosis in fibroblastoid cells. Mol Biol Cell *16*, 4473-4484.

3. Shaner, N.C., Campbell, R.E., Steinbach, P.A., Giepmans, B.N., Palmer, A.E., and Tsien, R.Y. (2004). Improved monomeric red, orange and yellow fluorescent proteins derived from Discosoma sp. red fluorescent protein. Nat Biotechnol *22*, 1567-1572.

4. Carl, U.D., Pollmann, M., Orr, E., Gertlere, F.B., Chakraborty, T., and Wehland, J. (1999). Aromatic and basic residues within the EVH1 domain of VASP specify its interaction with proline-rich ligands. Curr Biol *9*, 715-718.

5. Innocenti, M., Zucconi, A., Disanza, A., Frittoli, E., Areces, L.B., Steffen, A., Stradal, T.E., Di Fiore, P.P., Carlier, M.F., and Scita, G. (2004). Abi1 is essential for the formation and activation of a WAVE2 signalling complex. Nat Cell Biol *6*, 319-327.

6. Olazabal, I.M., Caron, E., May, R.C., Schilling, K., Knecht, D.A., and Machesky, L.M. (2002). Rho-kinase and myosin-II control phagocytic cup formation during CR, but not FcgammaR, phagocytosis. Curr Biol *12*, 1413-1418.

7. Jenzora, A., Behrendt, B., Small, J.V., Wehland, J., and Stradal, T.E. (2005). PREL1 provides a link from Ras signalling to the actin cytoskeleton via Ena/VASP proteins. FEBS Lett *579*, 455-463.

8. Baum, B., and Cherbas, L. (2008). Drosophila cell lines as model systems and as an experimental tool. Methods Mol Biol *420*, 391-424.

9. Rohn, J.L., Sims, D., Liu, T., Fedorova, M., Schöck, F., Dopie, J., Vartiainen, M.K., Kiger, A.A., Perrimon, N., and Baum, B. (2011). Comparative RNAi screening identifies a conserved core metazoan actinome by phenotype J Cell Biol *in press*.

10. Egile, C., Loisel, T.P., Laurent, V., Li, R., Pantaloni, D., Sansonetti, P.J., and Carlier, M.F. (1999). Activation of the CDC42 effector N-WASP by the Shigella flexneri IcsA protein promotes actin nucleation by Arp2/3 complex and bacterial actin-based motility. J Cell Biol *146*, 1319-1332.

11. Breitsprecher, D., Kiesewetter, A.K., Linkner, J., Urbanke, C., Resch, G.P., Small, J.V., and Faix, J. (2008). Clustering of VASP actively drives processive, WH2 domain-mediated actin filament elongation. Embo J *27*, 2943-2954.

12. Breuer, S., Gerlach, H., Kolaric, B., Urbanke, C., Opitz, N., and Geyer, M. (2006). Biochemical indication for myristoylation-dependent conformational changes in HIV-1 Nef. Biochemistry *45*, 2339-2349.

13. Schulte, A., Stolp, B., Schonichen, A., Pylypenko, O., Rak, A., Fackler, O.T., and Geyer, M. (2008). The human formin FHOD1 contains a bipartite structure of FH3 and GTPase-binding domains required for activation. Structure *16*, 1313-1323.

14. Breitsprecher, D., Kiesewetter, A.K., Linkner, J., Vinzenz, M., Stradal, T.E., Small, J.V., Curth, U., Dickinson, R.B., and Faix, J. (2011). Molecular mechanism of Ena/VASP-mediated actin-filament elongation. Embo J *30*, 456-467.